Non-contact Respiratory Rate Monitoring Based on the Principal Component Analysis

Hoda El Boussaki[1], Rachid Latif[2], Amine Saddik[3], Zakaria El Khadiri[4], Hicham El Boujaoui[5]
Laboratory of Systems Engineering and Information Technology LISTI, ENSA,
Ibn Zohr University, Agadir, Morocco[1,2,3,4,5]
Faculty of Applied Sciences, Ibn Zohr University, Ait Melloul, Morocco[3]

***Abstract*—Assessing respiratory rate is a critical determinant of one's health status. The proposed approach relies on principal component analysis (PCA) for the continuous monitoring of breathing rate using an RGB camera. This method employs remote plethysmography, a video-based technique enabling contactless tracking of blood volume fluctuations by detecting variations in pixel intensity on the skin. These pixels encompass the red, blue, and green channels, whose values, post-PCA dimensionality reduction, encode the signal containing vital information about the breathing rate. To assess the method's performance, it was tested on a group of seven volunteers, including individuals of both genders. The results reveal a Mean Absolute Deviation of 0.714 BPM and a Root Mean Square Error of 2.035 BPM when comparing the experimental measurements to the actual readings.**

***Keywords*—RGB; breathing rate; non-contact; principal component analysis; plethysmography**

I. Introduction

The respiratory rate is a vital indicator for the driver's current health state. It furnishes insights into clinical deterioration, offers predictive capabilities for cardiac arrest, and aids in the diagnosis of severe pneumonia. It exhibits sensitivity to various pathological conditions like cardiac events as well as stressors, including emotional stress, cognitive load, heat and cold [1]. Alterations and deviations in respiratory rate (RR) are not solely linked to respiratory disorders but also serve as a reliable indicator that a patient is facing challenges in maintaining homeostasis. Respiratory rate acts as an early and highly effective indicator of physiological conditions like hypoxia (insufficient cellular oxygen levels), hypercapnia (elevated carbon dioxide levels in the blood), as well as metabolic and respiratory acidosis. An adult's respiratory rate ranges between 12 and 20 breaths per minute [2]. At this specific respiratory rate, the elimination of carbon dioxide from the lungs matches the body's production of it. However, breathing rates that fall below 12 or exceed 20 may indicate a disturbance in the typical breathing patterns. According to recent findings, an adult who exhibits a respiratory rate exceeding 20 breaths per minute is likely to be in an unhealthy state, while an adult with a respiratory rate surpassing 24 breaths per minute is more likely to be in a critically ill condition [3].

The measurement of the respiratory rate is achieved using sensors, employing a technique that doesn't require direct contact. It quantifies the variation in the reflection of green, blue, and red light from the skin's surface, based on the distinction between specular and diffused reflections [4]. Remote plethysmography (rPPG) is a non-contact method widely used. It primarily comprises three components, a light source, human skin and a video camera. The light source illuminates the human skin, while the camera records the variations in color [5]. C. Massaroni at al. 2019 presented a method for monitoring the breathing pattern with an RGB camera. The changes in the pixels' intensity gives an overview on the variations of the chest's movements. The system has been tested on 12 volunteers. The Bland-Altman analysis revealed a bias of -0.01 breaths per minute, with respiratory rate values ranging from 10 to 43 breaths per minute [6]. Another method is to use thermal imaging as in the work proposed by Y. Takahashi et al. 2021. Their objective was to monitor the respiration of the subject by measuring temperature variations during exhalation and inhalation. To assess the proposed respiratory rate (RR) estimation method, a study was conducted on seven subjects. The results indicated a mean absolute error of 0.66 beats per minute (bpm) [7]. F. Yang et al. 2022 used an infrared thermal camera to estimate the respiratory rate. The nostril area was chosen as the region of interest and the changes in temperature give an indication on the breathing pattern. The absolute error between the estimated RR and the reference RR from all experiments is 1.47±1.33 breaths/min [8]. J. Kempfle et al. 2020 used a depth camera to estimate the respiratory rate. By capturing and monitoring the subtle changes in distance from the user's chest over time. The findings demonstrate that the method can accurately detect the breathing rate with a range of 92% to 97% from a distance of two meters [9]. P. S. Addison et al. 2023 also used a depth camera. The Bland-Altman analysis revealed limits of agreement of -1.42 to 1.36 breaths/min [10]. Z. El khadiri et al. 2023 proposed an efficient hybrid algorithm for non-contact physiological sign monitoring [11].

In our work, we propose an algorithm that monitors the respiratory rate through an RGB camera. The first part focuses on the face detection and the forehead extraction. The technique proposed by [12] was used for face detection and the extraction of the region of interest. Thus, the box blurring filter, the edge Sobel technique for edge detection, and morphological operations were employed. After that, The raw signal is obtained by computing the mean of each individual channel (red, green, and blue). The signal is then filtered to reduce the noise and the principal component analysis is applied to reduce dimentionality. The resulting signal is then filtered with a bandpass filter with cutoff frequencies of 0.5 and 0.1 Hz corresponding to the breathing rate. Finally, the respiratory rate is calculated by multiplying the maximum frequency after converting the signal to the frequency domain by 60. The summary of our contribution is the proposition of an approach for monitoring the respiratory rate using the

principal component analysis (PCA).

The organization of this paper is as follows: Section II provides an overview of recent advancements in contactless respiratory rate monitoring. Section III outlines our methodology. Subsequently, Section IV presents the results obtained from testing the method on diverse subjects. Finally, the conclusion summarizes the findings of this study and offers insights into future perspectives.

II. Related Work

Different methods exist to estimate the breathing rate. They are divided into two main categories that are non-contact methods and contact based methods. The first contact based method involves manual human counting. The second method utilizes a spirometer, which provides accurate measurements of respiratory parameters but can interfere with natural breathing and is not suitable for continuous RR monitoring. The third contact based approach involves capnometry but it requires contact with specialized equipment, which may not be comfortable for individuals [13]. Several contactless methods exist to monitor the respiratory rate through a camera. It can be thermal camera, a depth sensing camera or an RGB camera.

Observable fluctuations of the temperature in the region of interest (ROI) that is the nostril or the mouth area are generated by the process of inhalation and exhalation. Microelectromechanical sensors are utilized by thermal imaging cameras to generate images based on heat. The human body becomes distinct within the surrounding environment due to its higher heat emissions. P. Jakkaew et al. 2020 proposed a method that uses thermal imaging to monitor the respiratory rate [14]. The method obtained a root mean square error (RMSE) of 1.82±0.75 bpm. P. Jagadev et al. 2019 employed a thermal camera to monitor the temperature variations across the nostrils during the process of respiration [15]. To automate the tracking of the nostrils (region of interest) despite considerable head movement and object occlusion, a computer vision algorithm called "Ensemble of regression trees" is implemented. The algorithm had a precision of 98.76%. The algorithm demonstrated its effectiveness in managing both stationary and unpredictable head movements. A novel Breath Detection Algorithm (BDA) was introduced to differentiate between normal and abnormal breaths in the acquired breathing waveform. This was achieved by employing predefined thresholds, allowing the algorithm to determine the breaths and calculate the breaths per minute (BPM). A. Kwasniewska et al. 2019 used a Super Resolution (SR) Deep Learning (DL) network to generate enhanced thermal image sequences, which are subsequently analyzed. Despite the improved accuracy achieved through the application of SR algorithms, there is still a significant margin of error remaining [16]. C. B. Pereira et al. 2016 also used infrared thermography (IRT) to monitor the breathing rate. The algorithm takes into account not only the temperature variations around the mouth and nostrils but also the movements of both shoulders [17]. The method was tested in different conditions. The first one is normal breathing and the second one is when there is breathing disorders. During the first condition, a mean correlation of 0.98 and a root-mean-square error (RMSE) of 0.28 bpm was achieved. ON the other hand, the second condition reached a mean correlation of 0.95 and an RMSE of 3.45 bpm. Additionally, this also showcases the ability of IRT (Infrared Thermography) to effectively capture diverse breathing disorders. L. Chen et al. 2020 introduced a novel approach to non-contact breathing rate (BR) monitoring through a collaborative respiratory detection system. The system utilizes face and motion tracking methods simultaneously to achieve accurate monitoring of the breathing rate [18]. The algorithm showcases its remarkable accuracy with a root mean square error of 0.71 bpm and 0.76 bpm, along with a mean correlation of 0.97. M. Hu et al. 2018 used a combination of near-infrared and thermal imaging techniques for the measurements of breathing rate [19]. For tracking the region of interest (ROI) in thermal video, a tracking algorithm based on spatio-temporal context learning was employed.

In addition to the use of thermal imaging of the mouth and the nostrils, another method is the surveillance of the chest's movements. The expansion of the rib cage occurs during breathing as the diaphragm moves inward and outward. Monitoring the chest movements gives an indication on the number of breaths. In this case depth sensor can extract depth information of the chest area. W. Imano et al. 2020 estimated the respiratory rate from the depth value of the chest and the abdomen. The resulting respiratory rate was compared with the respiratory rate acquired using a spirometer. The experimental results demonstrated that the algorithm achieved a maximum error rate of 1.5% in estimating the respiratory rate [20]. A depth-sensing camera system was also assessed for its performance in continuously monitoring respiratory rate without the need for physical contact in the work of M. Mateu-mateus et al. 2019. The proposed algorithm involves detecting subject movements using optical flow algorithms on an infrared image. It then calculates the most appropriate region of interest (ROI) that can be utilized by the depth camera to capture the respiratory signal. The algorithm's validity was established by comparing it with a thorax plethysmography system, which served as a reference system [21]. M. Martinez et al. 2017 also used a depth camera to monitor the respiratory rate. The method demonstrates accuracy in 85.9% of the segments, which is comparable to the performance obtained from a chest sensor 88.7%. These results indicate that their use of computer vision is sufficiently precise for the given task.

The third type of cameras that can be used to monitor the breathing rate is RGB cameras. C. Romani et al. 2021 used an RGB camera. Their system enables automated tracking of chest movements associated with breathing, extracting the breathing signal through optical flow and RGB analysis methods. It eliminates events unrelated to breathing from the signal and identifies potential apneas. Additionally, it calculates the respiratory rate value every second [23]. H-S. Hwang et al. 2021 proposed a method for respiration measurement utilizing a region-of-interest detector based on machine learning, in addition to a clustering-based technique to estimate respiration pixels. The proposed approach comprises a model for classifying pixels based on their variance to determine if they convey respiration information. Additionally, a method is employed to classify pixels with distinct breathing components by analyzing the symmetry of the respiration signals [24]. It was established that the average error remained within approximately 0.1 breaths per minute (bpm). H. Ernst at al. 2022 used different combinations of RGB color channels using a hemispherical surface grid search method [25]. The grid search process led to the convergence towards the green channel in the baseline

modulation approach. M. Van Gastel et al. 2016 introduced a non-contact camera-based method for respiratory detection that is capable of operating in both visible and dark lighting conditions. The method relies on detecting the color variations of the skin induced by respiration [26].

III. Methodology

The pulsation of the heart generates fluctuations in arterial pressure as blood is pumped through the resistance of the vascular system. Due to the elasticity of arteries, their diameter changes in synchrony with these pressure variations. These alterations in blood volume lead to varying light absorption. Photoplethysmography (PPG) leverages this principle to optically measure blood volume changes by capturing reflected or transmitted light from illuminated skin, resulting in a PPG waveform [27]. When the face is captured, each frame consists of an image composed of three channels: red (R), green (G), and blue (B). The results obtained from Photoplethysmography (PPG) indicate that not only can pulsatility be determined, but also phase information regarding the cardiovascular waveform can be deduced from these three channels [28].

A. Region of Interest (ROI) Recognition

Fig. 1Face detection and ROI extraction. represents the face detection and the extraction of the region of interest algorithm proposed by H. El boussaki et al. 2023 [12].

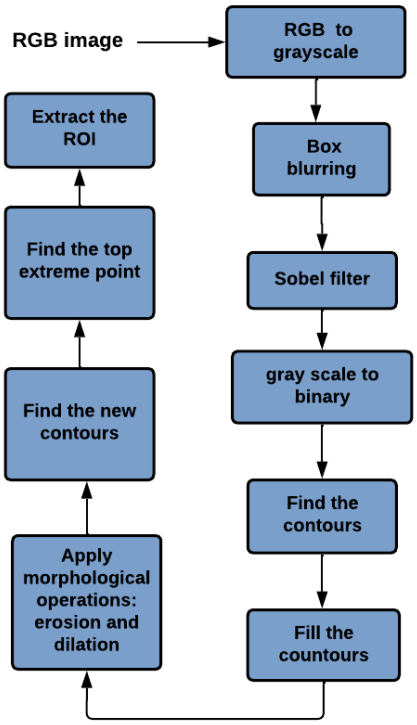

Fig. 1. Face detection and ROI extraction.

The process begins by converting the RGB image to grayscale and then applying a box blurring filter before using the Sobel filter. In the next step, the resulting image is transformed into a binary image, enabling contour detection. Once the contours are identified, the third step involves filling the interior of the contours with white and applying morphological operations. Finally, the last step involves locating new contours to determine the top extreme point, representing the top of the head. Fig. 1Face detection and ROI extraction. represented the diagram of the method proposed by [12]. After the top extreme point is detected a value is subtracted from the x coordinate of the top point, and another value is added to the y coordinate. This adjustment enables us to obtain a Region of Interest that starts slightly below the top of the head, precisely where the forehead is located.

B. Signal Extraction

The raw signal is obtained from the image by employing a function that computes the average of the pixels in each channel (red, green, and blue). The averages of these channels are then combined to form the signal. The RGB components within the region of interest (ROI) are spatially averaged across all pixels, resulting in an RGB component for each frame. These averaged RGB components form the raw signals. As new frames are processed, their values are added to the signal. At this point, the signal reflects the variations in pixel values from one frame to another.

C. Signal Filtering

The signal underwent additional denoising using a band-pass filter. This filter had a lower cutoff frequency of 0.1 Hz and a higher cutoff frequency of 0.5 Hz. When multiple channels are employed, the signal's dimensionality is commonly decreased by combining the channels in a linear manner. The Principal Component Analysis (PCA) is a well-known for its ability to reduce dimensionality. The PCA is applied on the filtered signal. It generates three linearly uncorrelated components, which are obtained by combining the three RGB signals in a linear fashion. The PCA is then a linear technique for reducing dimensionality, transforming a set of correlated features from a high-dimensional space into a sequence of uncorrelated features in a lower-dimensional space [29]. These uncorrelated features, known as principal components, are produced as a result [30]. It is a linear transformation that is orthogonal, indicating that all the principal components are perpendicular to one another. It reshapes the data in a manner where the first component endeavors to account for the highest amount of variance present in the original data. PCA aids in identifying the most prominent feature within a dataset, simplifies the representation of data in 2D and 3D plots, and facilitates the discovery of a sequence of linear combinations of variables [31]. The central aspect of PCA is dimensionality reduction, which involves reducing the number of dimensions within a given dataset. When the data exhibits a clear linear trend and directed points, applying PCA allows for straightforward reduction of the dimensional data into a lower-dimensional representation. The objective of PCA is to identify a new matrix that represents the principal components. This matrix captures the essential information and structure of the original data represented by X, an m × n matrix. Y is an m × n matrix that is connected through a linear transformation represented by P and is a re-representation of X as shown in Eq. (1) [32].

$$Y = PX \tag{1}$$

Where P represents the matrix that transforms Y into X.

Then the covariance of X is computed. The covariance quantifies the strength of the linear relationship between two variables. A high value indicates a strong positive relationship, while a low value suggests a weak or no relationship. It is represented in Eq. (2) [33].

$$C_x = \frac{1}{n-1} XX^T \tag{2}$$

Where C_x is the square symmetric matrix, the diagonal terms of C_x are the variance of particular measurement types and the off-diagonal terms of C_x are the covariance between measurement types.

C_x encompasses the correlations among all potential pairs of measurements, with the correlation values indicating the presence of noise and redundancy in our measurements. The objective is to acquire a matrix Y in such a way that the covariance matrix exhibits the highest variance. PCA operates under the assumption that P is an orthonormal matrix. Additionally, it assumes that the directions with the highest variances correspond to the most significant signals, making them the principal directions. C_y in terms of our variable P is represented in Eq. (3).

$$C_y = \frac{1}{n-1} YY^T = \frac{1}{n-1} PAP^T = \frac{1}{n-1} PXX^T P^T \tag{3}$$

C_y is a symmetric matrix, whose eigenvalues are arranged on the principal diagonal of the matrix A in descendent order, and the eigenvectors constitute the columns of the matrix P. The principal components of X are the eigenvectors of XX^T or the rows of P.Performing PCA on a dataset X involves subtracting the mean of each measurement type and then computing the eigenvectors of the matrix XX^T [33].

Fig. 2Signal filtering. represents the filtering algorithm and summarizes the previous steps. The signal goes through a denoising filter and a normalization, then a bandpass filter and the principal component analysis and a moving average filter.

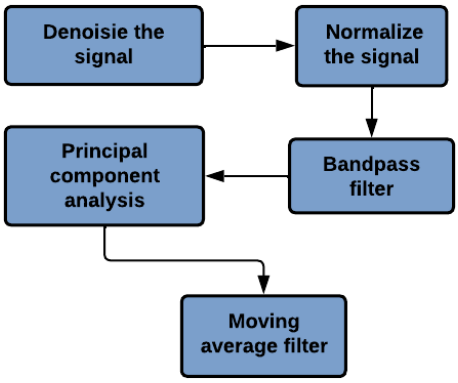

Fig. 2. Signal filtering.

Typically, the PCA technique uses tabular information and data, the rows stand in for the observations you want to incorporate and embed in a place with less dimensional space, while the columns correspond to the features for which you are looking for a reduced approximation. The principal components are generated by performing the singular value decomposition after the algorithm has calculated the covariance matrix in minute detail. Since smaller data sets are easier to examine, explore, visualize, and make analyzing data much easier and faster for machine learning algorithms without extraneous variables to process, the trick in dimensionality reduction is to trade a little accuracy for simplicity. For more convenience, the following pseudo-code illustrates the prominent steps for the Principal Component Analysis (PCA) technique:

Algorithm 1 Principal Component Analysis - PCA

Consider Z to be a data array of size nxm
Center and standardize the data array
Y $\leftarrow \frac{Z-\mu}{\sigma}$ while μ is the mean, and is the standard deviation
Calculate the covariance matrix of Y
Y $\leftarrow Y^T Y$
Calculate the eigenvectors and eigenvalues of $Y^T Y$
Sort the eigenvalues from largest to smallest $\lambda_1 > \lambda_2 > \ldots > \lambda_p$
Sort the eigenvectors in the matrix P accordingly
$Y^* \leftarrow YP$
Calculate the proportion of variance explained for each feature
Add features with the highest explained proportion of variation until it reaches a certain threshold

D. Respiratory Rate Estimation

A discrete Fourier transform is used to convert the resulting signal to the frequency domain [34]. The maximum of the frequency index is extracted as the frequency corresponding to the breathing. The respiratory rate is calculated with Eq. (4) [35]. The algorithm takes a sequence of images as input and identifies a Region of Interest (RoI). For each pixel within the region of interest, it constructs a trajectory in the time domain. This trajectory represents the pixel values across the entire sequence.

$$BPM = Max * 60 \tag{4}$$

Where Max is the maximum frequency
Fig. 3Respiratory rate estimation. represents the respiratory rate calculation algorithm. The discrete Fourier transform is applied to the signal. Then, if there is enough data and that means that the signal is large enough, the power spectrum with the highest magnitude is extracted. The value is used in Eq. (4) to calculate the respiratory rate.

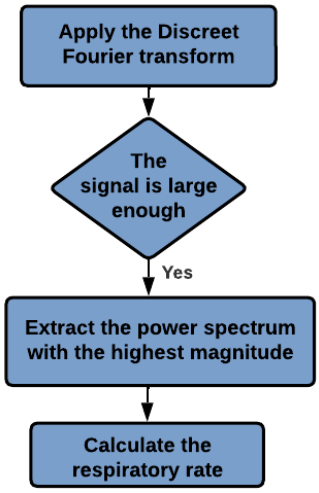

Fig. 3. Respiratory rate estimation.

IV. Experimental Results

A dataset was gathered, comprising seven volunteers, including four females and three males with a mean age of 37.8 years and an age range of 18 to 58 years. All participants provided informed consent for the test experiment. The volunteers was positioned at a distance of approximately 1 meter from the camera and instructed to blink and breathe naturally. This work was implemented on an Intel i7-1165G7 desktop using its camera. The respiratory rate was calculated through the proposed algorithm and compared with the values obtained by counting the number of breaths for one minute. In this paper, the performance of the respiratory rate measurement method is evaluated using the following indicators: the Mean Absolute Deviation (MAD) [36] and Root Mean Square Error (RMSE) [37]. The first metric represents the average absolute error between the estimated respiratory rate and the reference estimation. It provides insights into the accuracy of the measured respiratory rate compared to the desired respiratory rate and is calculated with Eq. (5) [38].

$$MAD = \frac{1}{n}\Sigma|RR^i_{rppg} - RR^i| \tag{5}$$

Where RRrppg is the respiratory rate estimated through an RGB camera and RR is the respiratory rate calculated manually. The second metric is calculated with equation 6 [38].

$$RMSE = \sqrt{\frac{\Sigma(RR^i_{rppg} - RR^i)^2}{n}} \tag{6}$$

Table IRespiratory Rate Obtained in Different Subjects represents the breathing rate obtained from seven volunteers that consists of three males and four females. The respiratory rate obtained using the method proposed was than compared with the respiratory rate acquired by counting the number of breaths per minute.

TABLE I. Respiratory Rate Obtained in Different Subjects

Subjects	Gender	Respiratory rate estimated (BPM)	Reference (BPM)
Subject 1	M	15	16
Subject 2	F	17	18
Subject 3	F	20	20
Subject 4	F	21	20
Subject 5	M	17	17
Subject 6	M	22	17
Subject 7	F	23	22

The evaluation metrics to assess the deviation of the measurement results from the reference breathing rate were employed to verify the accuracy of the measurement results. The calculated Mean Absolute Deviation (MAD) is 0.714 bpm and the calculated Root Mean Square Error is 2.035 bpm. Y. Takahashi et al. 2021 used a thermal camera and their method was tested on seven subjects with a mean absolute error of 0.66 beats per minute. Yang et al. 2022 used an infrared thermal camera and the absolute error is 1.47±1.33 breaths per minute. P. Jakkaew et al. 2020 proposed a method that uses a thermal camera and obtained a root mean square error of 1.82±0.75 bpm. C. B. Pereira et al. 2016 also used infrared thermography and achieved a root-mean-square error (RMSE) of 3.45 breaths per minute. C. Romano et al. 2021 used an RGB camera and obtained a bias of -0.03±1.38 bpm and -0.02±1.92 bpm in the Bland Altman analysis. H-S. Hwang and E. C. Lee 2021 proposed a method that was tested and evaluated using data from 14 men and women in a real-world environment using convolutional neural networks. During this evaluation, it was found that the correlation coefficient between the contactless signal and the reference signal being 0.93 on average indicates a strong positive linear relationship between the two signals. This suggests that our method's performance was quite accurate compared to others cited before. Our method gives a nearly same or an even higher performance compared to the use of other methods. However, the use of convolutional neural networks gives better performances.

V. Conclusion

This paper introduces a non-contact heart rate monitoring algorithm designed to measure the respiratory rate of the driver. The proposed method shows a Mean Absolute Deviation of 0.714 BPM and a Root Mean Square Error of 2.035 BPM. The approach consists of detecting the top extreme point of the head through image filtering, contour finding and morphological operations. When the top extreme point is detected, it is easy to determine the region of interest as it is located under the top extreme point. The signal is extracted from the changes in the pixels' intensity. Then, the signal is filtered and the principal component analysis is applied. Future works consist of evaluating the algorithm's processing time, improving it through parallel programming and implementing it in various embedded architectures.

ACKNOWLEDGMENT

We owe a debt of gratitude to the Ministry of National Education, Vocational Training, Higher Education and Scientific Research (MENF-PERSRS) and the National Center for Scientific and Technical Research of Morocco (CNRST) for their financial support (grant number: 27UIZ2022) and for the project Cov/2020/109.

REFERENCES

[1] A. Nicolò, C. Massaroni, E. Schena, and M. Sacchetti, "The importance of respiratory rate monitoring: From healthcare to sport and exercise," Sensors, 20(21), 6396, 2020.

[2] A. Rowden, "What is a normal respiratory rate based on your age?" January 2023.

[3] Respiratory rate. (n.d.). Physiopedia. https://www.physiopedia.com/Respiratory_Rate

[4] A. Bella, R. Latif, A. Saddik, and L. Jamad, "Review and Evaluation of Heart Rate Monitoring Based Vital Signs, A case Study: Covid-19 Pandemic," 6th IEEE Congress on Information Science and Technology (CiSt), 2020.

[5] A. Bella, R. Latif, A. Saddik, and F. Z. Guerrouj, "Monitoring of Physiological Signs and Their Impact on The Covid-19 Pandemic: Review. E3S Web of Conferences, 229, 01030, 2021.

[6] C. Massaroni, D. Lo Presti, D. Formica, S. Silvestri, and E. Schena, "Non-Contact monitoring of breathing pattern and respiratory rate via RGB signal measurement," Sensors, 19(12), 2758, 2019.

[7] Y. Takahashi, Y. Gu, T. Nakada, R. Abe, and T. Nakaguchi, T, "Estimation of Respiratory Rate from Thermography Using Respiratory Likelihood Index," Sensors, 21(13), 4406, 2021.

[8] F. Yang, S. He, S. Sadanand, A. Yusuf, and M. Bolic, "Contactless measurement of vital signs using thermal and RGB cameras: A study of COVID 19-Related Health Monitoring," Sensors, 22(2), 627, 2022.

[9] J. Kempfle, and K. Van Laerhoven, "Towards breathing as a sensing modality in Depth-Based Activity recognition," Sensors, 20(14), 3884, 2020.

[10] P. S. Addison, A. Antunes, D. Montgomery, P. Smit, and U. R. Borg, "Robust Non-Contact Monitoring of Respiratory Rate using a Depth Camera," Journal of Clinical Monitoring and Computing, 2023.

[11] Z. El Khadiri, R. Latif, and A. Saddik, "An efficient hybrid algorithm for non-contact physiological sign monitoring using plethysmography wave analysis," Computer Methods in Biomechanics and Biomedical Engineering. Imaging & Visualization, 1–17, 2023.

[12] H. El Boussaki, R. Latif, and A. Saddik, "Video-based Heart Rate Estimation using Embedded Architectures," International Journal of Advanced Computer Science and Applications, 14(5), 2023.

[13] M. C. T. Manullang, Y. Lin, S. Flaxman,and N. Chou, "Implementation of Thermal Camera for Non-Contact Physiological Measurement: A Systematic Review," Sensors, 21(23), 7777, 2021.

[14] P. Jakkaew and T. Onoye, "Non-Contact Respiration Monitoring and Body Movements Detection for Sleep Using Thermal Imaging," Sensors (Basel). 2020 Nov 5;20(21):6307.

[15] P. Jagadev, and L. I. Giri, "Non-contact monitoring of human respiration using infrared thermography and machine learning," Infrared Physics & Technology, 104, 103117, 2020.

[16] A. Kwasniewska, M. Szankin, J. Ruminski, and M. Kaczmarek, M. "Evaluating Accuracy of Respiratory Rate Estimation from Super Resolved Thermal Imagery," 2029.

[17] C. B. Pereira, X. Yu, M. Czaplik, V. Blazek, B. Venema, and S. Leonhardt, "Estimation of breathing rate in thermal imaging videos: a pilot study on healthy human subjects," Journal of Clinical Monitoring and Computing, 31(6), 1241–1254, 2016.

[18] L. Chen, M. Hu, N. Liu, G. Zhai, and S. X. Yang, "Collaborative use of RGB and thermal imaging for remote breathing rate measurement under realistic conditions," Infrared Physics & Technology, 111, 103504, 2020.

[19] M. Hu, G. Zhai, B. Yang, Y. Fan, H. Duan, W. Zhu, and M. Yang, "Combination of near-infrared and thermal imaging techniques for the remote and simultaneous measurements of breathing and heart rates under sleep situation," PLOS ONE, 13(1), e0190466, 2018.

[20] W. Imano, K. Kameyama, M. Hollingdal, J. C. Refsgaard, K. S. Larsen, C. S. R.Topp, S. H. Kronborg, J. D. Gade, and B. Dinesen, "Non-Contact respiratory measurement using a depth camera for elderly people," Sensors, 20(23), 6901, 2020.

[21] M. Mateu-Mateus, F. Guede-Fernandez, M. A. Garcia-Gonzalez, J. Ramos-Castro, and M. Fernandez-Chimeno, "Non-Contact Infrared-Depth Camera-Based method for respiratory rhythm measurement while driving," IEEE Access, 7, 152522–152532, 2019.

[22] M. Martínez, and R. Stiefelhagen, "Breathing Rate Monitoring during Sleep from a Depth Camera under Real-Life Conditions," 2017.

[23] C. Romano, E. Schena, S. Silvestri, and C. Massaroni, "Non-Contact respiratory monitoring using an RGB camera for Real-World applications," Sensors, 21(15), 5126, 2021.

[24] H-S. Hwang, and E. C. Lee, "Non-Contact Respiration Measurement method based on RGB camera using 1D convolutional neural networks," Sensors, 21(10), 3456, 2021.

[25] H. Ernst, H. Malberg and M. Schmidt, "Non-contact Measurement of Respiration Rate with Camera-based Photoplethysmography During Rest and Mental Stress," 2022 Computing in Cardiology (CinC), Tampere, Finland, pp. 1-4, 2022.

[26] M. Van Gastel, S. Stuijk, and G. De Haan, "Robust respiration detection from remote photoplethysmography," Biomedical Optics Express, 7(12), 4941, 2016.

[27] Z. El Khadiri, R. Latif, and A. Saddik, "Breathing pattern assessment through the empirical mode decomposition and the empirical Wavelet transform algorithms," In Lecture notes on data engineering and communications technologies, pp. 262–271, 2023.

[28] W. Verkruysse, L. O. Svaasand,and J. M. Nelson, "Remote plethysmographic imaging using ambient light," Optics Express, 16(26), 21434, 2008.

[29] Z. El Khadiri, R. Latif, and A. Saddik, "Remote heart rate measurement using plethysmographic wave analysis," In Lecture notes in networks and systems, pp. 254–267, 2023.

[30] K. Parte, "Dimensionality reduction: principal component analysis," Medium, December 2021.

[31] V. Lendave, "Detecting Orientation of Objects in Image using PCA and OpenCV," Analytics India Magazine, 2021.

[32] E. De Benedetto, A. Bottiglieri, S. Pisa, and M. Cavagnaro, "Cardiorespiratory frequency monitoring using the principal component analysis technique on UWB Radar Signal," International Journal of Antennas and Propagation, 1–6, 2017.

[33] J. Shlens, "A tutorial on principal component analysis," 2003.

[34] S. Mejhoudi, R. Latif, W. Jenkal, A. Saddik, and A. El Ouardi, "Hardware Architecture for Adaptive Dual Threshold Filter and Discrete Wavelet Transform based ECG Signal Denoising," International Journal of Advanced Computer Science and Applications, 12(11), 2021.

[35] H. El Boussaki, R. Latif, and A. Saddik, "A review on Video-Based Heart Rate, Respiratory Rate and Blood Pressure Estimation," In Lecture notes in networks and systems, pp. 129–140, 2023. H. El Boussaki, R. Latif, and A. Saddik, "A review on Video-Based Heart Rate, Respiratory Rate and Blood Pressure Estimation," In Lecture notes in networks and systems, pp. 129–140, 2023.

[36] O. E. B'charri, R. Latif, K. Elmansouri, A. Abenaou, and W. Jenkal, "ECG signal performance de-noising assessment based on threshold tuning of dual-tree wavelet transform," Biomedical Engineering Online, vol. 16, no. 1, Feb. 2017.

[37] W. Jenkal, R. Latif, A. Toumanari, A. Dliou, O. E. B'charri, and F. M. R. Maoulainine, "An efficient algorithm of ECG signal denoising using the adaptive dual threshold filter and the discrete wavelet transform," Biocybernetics and Biomedical Engineering, vol. 36, no. 3, pp. 499–508, Jan. 2016.

[38] B. Zhang, H. Li, L. Xu, L. Qi, Y.-D. Yao, and S. E. Greenwald, "Noncontact heart rate measurement using a webcam, based on joint blind source separation and a skin reflection model: for a wide range of imaging conditions," Journal of Sensors, vol. 2021, pp. 1–18, Jul. 2021.